Quantitative mitochondrial redox imaging of breast cancer metastatic potential

He N. Xu
University of Pennsylvania
School of Medicine
Department of Radiology
B6 Blockley Hall
423 Guardian Drive
Philadelphia, Pennsylvania 19104-6069

Shoko Nioka
University of Pennsylvania
School of Medicine
Department of Biochemistry and Molecular Biophysics
Johnson Research Foundation
250 Anatomy-Chemistry Building
3620 Hamilton Walk
Philadelphia, Pennsylvania 19104-6059

Jerry D. Glickson
University of Pennsylvania
School of Medicine
Department of Radiology
B6 Blockley Hall
423 Guardian Drive
Philadelphia, Pennsylvania 19104-6069

Britton Chance
University of Pennsylvania
School of Medicine
Department of Biochemistry and Molecular Biophysics
Johnson Research Foundation
250 Anatomy-Chemistry Building
3620 Hamilton Walk
Philadelphia, Pennsylvania 19104-6059

Lin Z. Li
University of Pennsylvania
School of Medicine
Department of Radiology
B6 Blockley Hall
423 Guardian Drive
Philadelphia, Pennsylvania 19104-6069

Abstract. Predicting tumor metastatic potential remains a challenge in cancer research and clinical practice. Our goal was to identify novel biomarkers for differentiating human breast tumors with different metastatic potentials by imaging the *in vivo* mitochondrial redox states of tumor tissues. The more metastatic (aggressive) MDA-MB-231 and less metastatic (indolent) MCF-7 human breast cancer mouse xenografts were imaged with the low-temperature redox scanner to obtain multi-slice fluorescence images of reduced nicotinamide adenine dinucleotide (NADH) and oxidized flavoproteins (Fp). The nominal concentrations of NADH and Fp in tissue were measured using reference standards and used to calculate the Fp redox ratio, $Fp/(NADH+Fp)$. We observed significant core-rim differences, with the core being more oxidized than the rim in all aggressive tumors but not in the indolent tumors. These results are consistent with our previous observations on human melanoma mouse xenografts, indicating that mitochondrial redox imaging potentially provides sensitive markers for distinguishing aggressive from indolent breast tumor xenografts. Mitochondrial redox imaging can be clinically implemented utilizing cryogenic biopsy specimens and is useful for drug development and for clinical diagnosis of breast cancer. © *2010 Society of Photo-Optical Instrumentation Engineers.* [DOI: 10.1117/1.3431714]

1 Introduction

Cancer metastasizes through hematogenous and lymphatic pathways to distant organs.[1] Metastasis is the final step of cancer progression and remains the primary cause of death from solid tumors.[1,2] The tendency of a primary tumor to form secondary metastatic lesions is the metastatic potential of that tumor.[3] Knowledge of tumor metastatic potential may help physicians to select a proper level of treatment based on tumor aggressiveness while avoiding unnecessary side effects on patients.[4] Due to the complexity of cancer, such as inter- and intratumoral heterogeneity[5–9] in structure, gene expression, and metabolism, predicting tumor metastatic potential remains a major challenge in cancer research and clinical practice. Current clinical metastatic prognosis for breast cancer is based on factors including tumor size, stage, grade, and other histopathological information from localized biopsy samples. However, it is still difficult to accurately predict the likelihood that a specific breast tumor in a specific patient will produce a distant metastasis. As a result, some low-grade breast tumors that have been treated less aggressively may disseminate, while some high-grade tumors that were treated aggressively may be nonmetastatic in nature.

Address all correspondence to Lin Z. Li, Department of Radiology, School of Medicine, University of Pennsylvania, B6 Blockley Hall, 423 Guardian Drive, Philadelphia, PA 19104-6069. Tel: 215-222-1888; Fax: 215-573-2113; E-mail: linli@mail.med.upenn.edu

Imaging techniques that measure the spatial distribution of physiological parameters, i.e., image the heterogeneity of tumor metastatic biomarkers, may prove useful and necessary for predicting tumor metastatic potential. Many processes are associated with tumor aggressiveness, such as glucose metabolism, hypoxia, angiogenesis, and the activity of matrix metalloproteinases (MMPs) within the tumor microenvironment. A variety of clinical and preclinical methods that image one or more indices of these phenomena have been reviewed.[3]

In this study, we employed the mitochondrial redox scanning technique to distinguish between aggressive and indolent human breast tumor mouse xenografts. Redox scanning developed by Chance and collaborators[10–13] utilizes a cryogenic nicotinamide adenine dinucleotide (NADH)/flavoproteins fluorescence imaging instrument to image the mitochondrial redox state in biological samples snap-frozen under liquid nitrogen. The light emissions originate from the two major classes of intrinsic fluorophores in tissue, NADH and oxidized flavoproteins (Fp) containing flavin adenine dinucleotide (FAD), whose fluorescence intensities are enhanced 10-fold at liquid nitrogen temperature.[14] NADH and $FADH_2$ are energy carrying co-enzymes, which are fed into the electron transport chain in mitochondria to generate adenosine-5′-triphosphate (ATP) by oxidative phosphorylation. It has been shown that Fp and NADH are sensitive indicators of mitochondrial metabolic states,[14–25] and their ratio is related to the hydroxybutyrate/acetoacetate ratio and thus to the NAD^+-coupled mitochondrial redox potential $NAD^+/NADH$ and to the thermodynamic potential ΔG of the mitochondrial system.[14,26] A highly active mitochondrial metabolic state results in oxidation of the electron transport system, leading to decreases in NADH and increases in Fp, which result in increases in the Fp redox ratio (or shortened as Fp ratio), $Fp/(Fp+NADH)$.

In our previous study[27] directed at predicting the metastatic potential of five human melanoma mouse xenografts that spanned the full range of tumor aggressiveness, we used the redox scanning technique to identify a distinctly more oxidized core region in aggressive tumors. We demonstrated that the invasive potential of all five melanoma lines measured in a Boyden chamber varied linearly with the oxidized redox ratio of the cores of these tumors. However, prediction of metastatic potential in melanoma is clinically less critical than in other malignancies such as prostate and breast cancer because melanoma is almost invariably surgically excised, and the aggressiveness of melanoma can be judged by its histological characteristics as well as by the vertical height of the tumor.[28] However, melanoma serves well as a starting point for establishing biomarkers of metastatic potential because a wide range of human tumor lines with varying metastatic potential measured in culture and *in vivo* are available.[29–32]

Our goal in the present study is to apply mitochondrial redox scanning to human breast cancer mouse xenograft models and investigate whether redox imaging biomarkers can distinguish between the aggressive and the indolent breast cancers. Here we report the results obtained for two groups of human breast tumor mouse xenografts: the highly metastatic (aggressive) tumor MDA-MB-231 and the poorly metastatic (indolent) MCF-7.[33] These results indicate that several redox imaging biomarkers can differentiate between MDA-MB-231 and MCF-7 tumors. This study also allows us to conduct a preliminary comparison of low-temperature fluorescence data on aggressive and indolent forms of breast cancer with the previous more extensive study on melanoma that combined fluorescence with magnetic resonance imaging (MRI) and histopathological data to distinguish between aggressive and indolent forms of melanoma. This analysis suggests that the conclusions regarding mitochondrial redox states drawn from the melanoma study appear to apply also to breast cancer. Thus, the success of this study as well as our previous melanoma study support the utility of the mitochondrial redox state as a possible biomarker for tumor metastatic potential. These results may allow us to develop clinically translatable noninvasively detectable redox imaging biomarkers for predicting the metastatic potential of breast cancer and perhaps other solid tumors.

2 Materials and Methods

2.1 Mouse Xenograft Model and Sample Preparation

The animal protocol utilized in these studies was approved by the Institutional Animal Care and Use Committee of the University of Pennsylvania. The human breast cancer cells (the aggressive MDA-MB-231 and the indolent MCF-7) were propagated in RPMI1640 medium supplemented with 10% fetal bovine serum. Breast cancer cells ($\sim 1 \times 10^7$, 100 μl) were subcutaneously implanted into the upper thighs of the hind legs of 4- to 5-week-old female athymic nude mice (strain NCr-nu/nu) obtained from the U.S. National Cancer Institute. An estrogen pellet (0.72 mg, 60 days) was implanted subcutaneously in the mouse chest using a 10-gauge trocar immediately before MCF-7 inoculation. Tumors were allowed to grow to 6 to 10 mm in diameter measured with calipers. Tumor volume was estimated as $1/2ab^2$ (mm^3), where a is the length of the long axis and b is the length of the short axis along two perpendicular directions in the tumor. The tumor-bearing mice were then anesthetized with ketamine/acepromazine (100/10 mg/Kg) and snap-frozen under liquid N_2 so that the *in vivo* metabolic states of the tumors were preserved. The frozen tumors were then excised with a handsaw in a low-temperature environment and kept under liquid N_2.

The sample preparation details for performing redox scanning have been reported elsewhere.[12,34] Briefly, each frozen tumor was mounted in liquid N_2–chilled mounting buffer (H_2O:ethanol:glycerol=10:30:60, freezing point -30 °C) with two snap-frozen reference standards (one NADH and one FAD, powder diluted in 10 mM Tris-HCl buffer made from a 1 M pH7 buffer solution, concentration FAD $=719$ μM, NADH$=1318$ μM) mounted adjacent to the tumor and maintained at low temperature. Such prepared samples were stored under liquid N_2 for redox scanning.

2.2 Redox Scanning

The testing and operation of the redox scanner used for this study have been previously described.[10–12] Briefly, we milled the sample surface flat under liquid nitrogen utilizing the grinder component of the scanner. Milling away layer after layer of surface tissue exposed tissue sections at various depths from the original surface of the tumor. Fluorescence scanning with a bifurcated fiber-optic probe about 70 μm
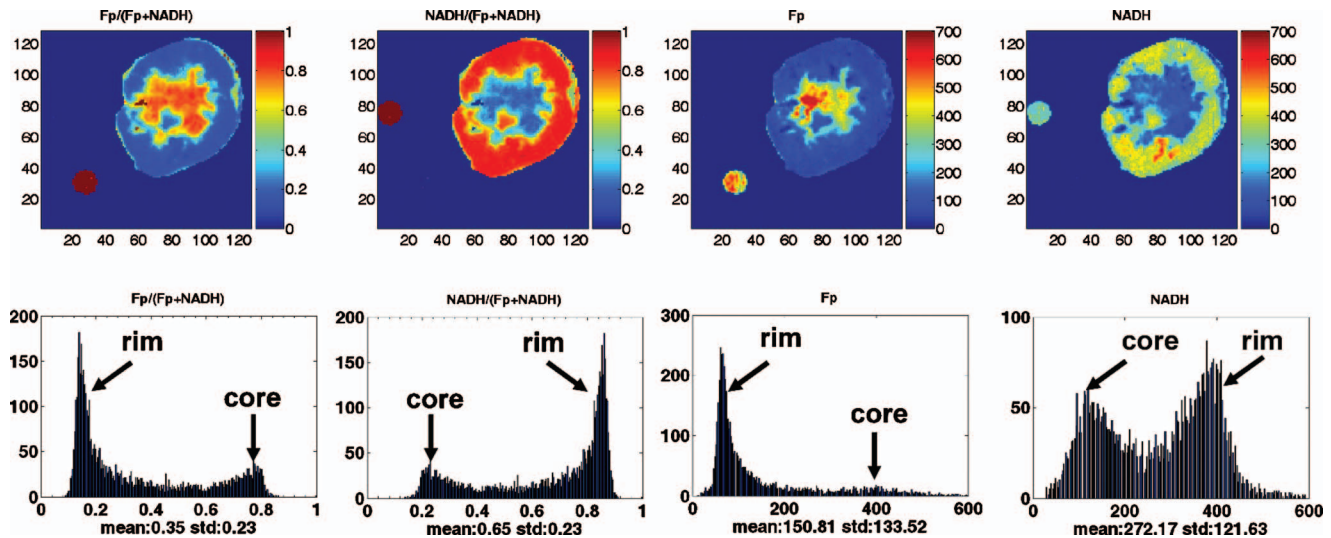
Fig. 1 Typical pseudo-color redox images and their corresponding histograms of highly metastatic human breast tumor MDA-MB-231 mouse xenografts (tissue section depth 1740 μm). The color bars of the Fp and NADH images indicate the nominal concentrations in μM relative to the corresponding snap-frozen solution standards, and the color bar of the Fp and NADH ratio image indicates the ratio range from 0 to 1. Note that by definition, NADH ratio is merely $1-($Fp ratio$)$. The x axes of the histograms represent the Fp or NADH redox ratio or concentration. The y axes represent the number of pixels in the tumor section having a specific value of Fp or NADH redox ratio or nominal concentration. The small round spots outside the tumor section are the images of Fp or NADH reference standards. The peaks corresponding to tumor core or rim are labeled in the histograms. The image matrix was 128×128, and the step size was 100 μm.

above the flat surface then generated redox images of the tumor section. The Fp excitation and emission channel filters were centered at 430 nm $\pm$ 25 nm and 525 nm $\pm$ 32 nm, respectively; the NADH excitation and emission channel filters were centered at 360 nm $\pm$ 26 nm and 430 nm $\pm$ 25 nm, respectively. A short-pass glass filter (transmitting light at 472 nm $\pm$ 84 nm, with O.D. 4.5 out-of-band rejection for light with wavelengths of 640 nm or longer) was used in the NADH channel to prevent red light leakage, yielding total out-of-band rejection of O.D. 7.5 for red light. A neutral density filter was inserted in the emission channel when the signal was saturated. Filters were rotated by spinning filter wheels. The NADH and Fp emission signals were transmitted to a photomultiplier tube (PMT, R928 from Hamamatsu, Inc.; sensitivity range: 185 to 900 nm) and processed on a PC to construct the fluorescence images of the scanned sample section.

The typical scanning matrix for this study was 128×128, with a step size of 100 or 200 μm. Images of tissue sections at three to five different depths from tumor top surface with a separation of 200 to 400 μm were obtained for each tumor, resulting in 15 imaging sections in total for four MCF-7 tumors and 9 sections for three MDA-MB-231 tumors.

2.3 Data Analysis

The images were analyzed with MATLAB software to generate the mean value and the standard deviation of the fluorescence signal with the signal intensity corrected for neutral density filters if they were used in any channel. For reference standards, the area inside each reference tube was selected as the region of interest (ROI). The mean value of the signal intensity from each ROI of the reference tube was computed by subtraction of the background signal of the blank. The NADH tube serves as the blank for the FAD tube and vice versa. For tissue the ROI was drawn excluding the mouse

skin. The nominal NADH and Fp concentrations in the tissue were calculated by comparing the tissue signal intensity with the mean signal intensity of the reference standards.

The processed redox images are displayed with a color bar on the right side of each image indicating the range of data values (Figs. 1 and 2). The NADH or Fp images are displayed in units of concentration (μM); the value of the redox ratio images ranges between 0 and 1. A histogram for the region of interest in an image was generated by counting the number of pixels exhibiting each specific value of NADH or Fp nominal concentration or Fp redox ratio.

All histograms of indolent MCF-7 tumors have only one major peak. For the aggressive MDA-MB-231 tumors, histograms of each image section usually exhibit a two-peak bimodal distribution for the Fp redox ratio and Fp and NADH concentrations, corresponding to a core-rim difference. The tumor core is defined as the region with higher Fp redox ratio corresponding to a more oxidized state and is usually located in the central region of the aggressive tumor section. The average values of the Fp redox ratio and Fp and NADH concentrations of the tumor core in each tumor section were obtained from the peaks on the right side of the histograms (read to two significant digits). They were then averaged across multiple image sections of each tumor to obtain the mean values of the entire tumor, denoted by Fp ratio (core), Fp (core), and NADH (core), respectively. In the same way, analyses were conducted by measuring the left-hand peaks in the histograms to obtain Fp ratio (rim), Fp (rim), and NADH (rim) denoting the mean value in the rim of the entire tumor, respectively. For both the aggressive and the indolent tumors, the mean values of the Fp and NADH concentration and the Fp ratio were also calculated for each tumor section. They were then averaged across multiple sections of each tumor to obtain the mean values of the entire tumor, denoted by Fp
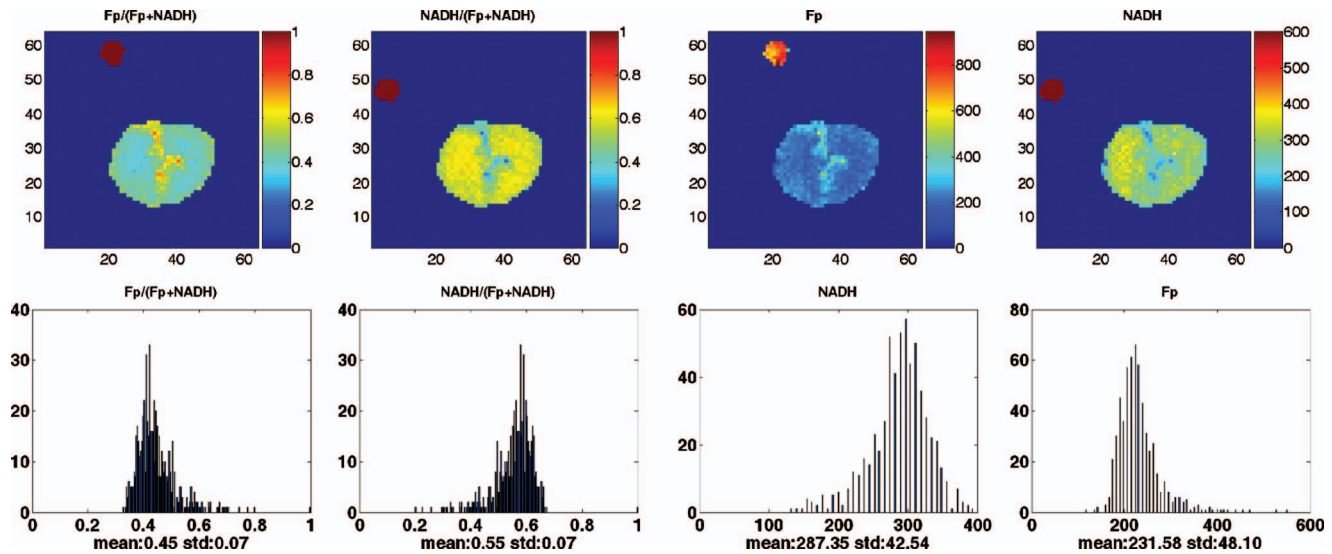
Fig. 2 Typical redox images and corresponding histograms of indolent human breast tumor MCF-7 mouse xenografts (tissue section depth 980 μm). The x axes of the histograms represent the Fp or NADH redox ratio or nominal concentration. The y axes represent the number of pixels in the tumor section having a specific value of Fp or NADH redox ratio or nominal concentration. The small round spots outside the tumor section are Fp or NADH reference standards. The image matrix was 128×128, and the step size was 200 μm (twice that of the pixel size of MDA-MB-231 xenograft images in Fig. 1).

ratio (mean) for the redox ratio or Fp (mean) and NADH (mean) for the concentration.

Each of the indices defined earlier were then averaged across three to four tumors for each tumor line to obtain the mean values and standard deviations (SDs) for the tumor line which are reported in Tables 1 and 2.

For the aggressive MDA-MB-231 tumors, in order to determine whether there exists a significant core-rim difference, a two-tail paired t-test was performed to compare the average Fp ratio (core) and Fp ratio (rim) in each tumor. The same comparison was made between Fp (core) and Fp (rim) as well as between NADH (core) and NADH (rim).

To identify biomarkers distinguishing the aggressive from the indolent tumors, six indices of Fp from three MDA-MB-231 tumors, i.e., Fp ratio (core), Fp ratio (rim), Fp ratio (mean), Fp (core), Fp (rim), and Fp (mean), were compared, respectively, with the Fp ratio (mean) and Fp (mean) from four MCF-7 tumors using a two-tail unpaired t-test assuming unequal variance. In the same way, three indices of NADH from the MDA-MB-231, NADH (core), NADH (rim), and

NADH (mean) were compared with NADH (mean) of MCF-7, respectively ($p < 0.05$ was considered as statistically significant).

3 Results

3.1 Significant Core-Rim Differences Detected in the Aggressive Breast Tumors but Not in the Indolent Breast Tumors

Figures 1 and 2 display typical redox images of the aggressive MDA-MB-231 and the indolent MCF-7 breast tumors, respectively. As shown in Fig. 1, distinct differences between the tumor core and rim were observed for all aggressive MDA-MB-231 breast tumors, where the core is defined as the more oxidized region with the higher Fp redox ratio, Fp/(Fp +NADH). The typical histograms of the aggressive tumor images show the bimodal pattern with two widely separated peaks. The right peak in the Fp redox ratio histogram corresponds to the more oxidized tumor core region and the left peak to the more reduced rim region. The average Fp ratio (core)$=0.81 \pm 0.02$, and the average Fp ratio (rim) $=0.30 \pm 0.18$ ($p=0.03$) for the MDA-MB-231 tumor line (Table 1). There is also a statistically significant difference between core and rim with respect to Fp concentration ($p =0.02$), but the core-rim difference for NADH has borderline significance ($p=0.08$; Table 2) probably because of the limited sample size. Such distinct core and rim differences were not observed for the indolent MCF-7 breast tumors as shown in Fig. 2. Therefore, only the average Fp ratio (mean) was calculated to be 0.42 ± 0.03 with a standard deviation smaller than that of the Fp ratio (mean) for the more aggressive MDA-MB-231 line, 0.46 ± 0.11 (Table 1). The aggressive tumors were more heterogeneous than the indolent tumors in spite of having a comparable mean Fp ratio ($p=0.65$). Note that the average tumor sizes of two tumor lines

Table 1 The Fp redox ratios of the two tumor groups.

	Fp ratio (mean)	Fp ratio (core)	Fp ratio (rim)
MDA-MB-231	0.46±0.11	0.81±0.02	0.30±0.18
MCF-7	0.42±0.03		
P value (core-rim)[a]		0.03	
P value (between lines)[b]	0.65	0.00001	0.35

[a]Comparing the Fp ratio (core) and the Fp ratio (rim) of the MDA-MB-231 tumors.
[b]Comparing the three Fp ratios of the MDA-MB-231 tumors with the Fp ratio (mean) of the MCF-7 tumors.

Table 2 The nominal concentration of NADH and Fp in μM relative to NADH or Fp reference standards.

	NADH (mean)	NADH (core)	NADH (rim)	Fp (mean)	Fp (core)	Fp (rim)
MDA-MB-231	206±96	89±35	312±147	166±36	497±121	91±27
MCF-7	318±89			255±27		
P value (231 core-rim)[a]		0.08			0.02	
P value between lines[b]	0.19	0.009	0.96	0.03	0.07	0.0008

[a]Comparing the NADH or Fp nominal concentrations in the core with those in the rim of the MDA-MB-231 tumors.
[b]Comparing the nominal concentrations of NADH and Fp of the MDA-MB-231 tumors with the average nominal concentrations of NADH and Fp in the MCF-7 tumors, respectively.

(173 ± 102 mm^3 for MDA-MB-231 and 165 ± 106 mm^3 for MCF-7, $p=0.96$) were comparable.

3.2 Several Biomarkers Distinguish the Aggressive from the Indolent Breast Tumors

As delineated in Fig. 3(a) and Table 1, the Fp ratio (core) of MDA-MB-231 tumors is significantly different from the Fp ratio (mean) of MCF-7 line ($p=0.00001$), whereas the Fp ratio (rim) and Fp ratio (mean) of the aggressive tumors fail to differ significantly from the Fp ratio (mean) of the indolent tumors ($p>0.05$). In addition to the Fp ratio (core), several indices of NADH and Fp nominal concentrations such as NADH (core), Fp (rim), and Fp (mean) are also biomarkers of the aggressive MDA-MB-231 breast tumors [Figs. 3(b) and 3(c) and Table 2]. The average of NADH (core) in the aggressive MDA-MB-231 tumor line was 89 ± 35 μM, while the average of NADH (mean) in the MCF-7 tumor line was 318 ± 89 μM. The former parameter is significantly lower ($p=0.009$). The difference between the average Fp (core) in MDA-MB-231(497 ± 121 μM) and the average Fp (mean) in MCF-7 (255 ± 27 μM) has borderline statistical significance ($p=0.07$). The average concentration of NADH (rim) in the aggressive MDA-MB-231 tumor line was 312 ± 147 μM, which did not significantly differ from NADH (mean) in MCF-7 ($p=0.96$). However, Fp (rim) in the aggressive tumors (91 ± 27 μM) differed significantly from Fp (mean) in the indolent ones ($p=0.0008$). Fp (mean) can also distinguish

between the aggressive and indolent tumors with statistical significance, but NADH (mean) cannot ($p=0.03$ versus 0.19). Thus, NADH (core), Fp (rim), Fp (mean), and potentially Fp (core) may also serve as potential biomarkers for distinguishing between aggressive and indolent breast tumors in addition to Fp ratio (core).

4 Discussion

4.1 Characteristic Core-Rim Pattern of the Aggressive Breast Tumors and Their Redox State Indices Distinguish between Aggressive and Indolent Breast Tumors

We have employed redox scanning to characterize two breast cancer mouse xenograft lines, the aggressive (highly metastatic) MDA-MB-231 and the indolent (poorly metastatic) MCF-7. As indicated by our redox imaging results, significant core-rim differences were observed in the aggressive breast tumors, but the indolent tumors were relatively uniform. The average value of the Fp ratio (core)—the Fp redox ratio of the aggressive tumor core—but not the average Fp ratio (mean)—the Fp redox ratio of the entire tumor—differentiates between the aggressive and indolent breast tumor lines. This is consistent with our previous imaging study of human melanoma mitochondrial redox state,[27] clearly demonstrating the ability of redox imaging to map the heterogeneity of tumors and to distinguish between aggressive and indolent phenotypes of
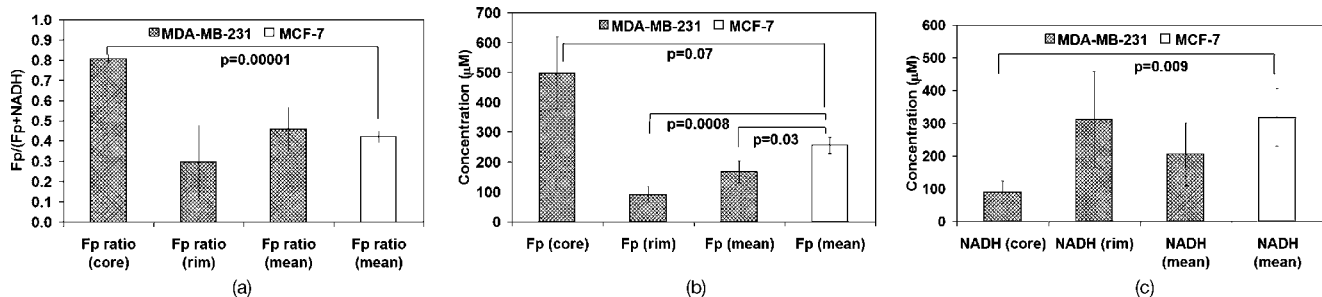

Fig. 3 Redox imaging biomarkers distinguish between the MDA-MB-231 (aggressive, solid bars) tumor line and the MCF-7 (indolent, open bars) tumor line. Figure 3(a) shows that only the average of the Fp ratio (core) of the aggressive tumors can distinguish the aggressive from the indolent lines. Figures 3(b) and 3(c) show the average concentrations of Fp and NADH relative to the frozen-solution standards for the two tumor groups, respectively. Since there is no distinct core-rim difference identified for the MCF-7 tumors, only the average values of Fp (mean), NADH (mean), and Fp ratio (mean) of the tumor lines were plotted for the preceding figures.
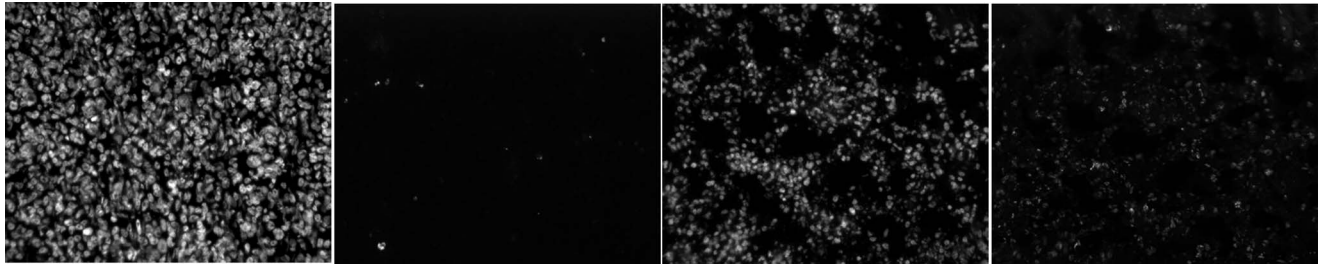
Fig. 4 TUNEL assays for tumor cell death in a representative MDA-MB-231 tumor. From left to right: tumor rim DAPI staining, tumor rim FITC staining, tumor core DAPI staining, and tumor core FITC staining. DAPI stains the cell nucleus, and FITC stains the TUNEL positive cells (Ref. [37]).

both melanoma and breast cancer tumor lines.

The nominal concentration images of NADH and Fp obtained by comparing tissue fluorescence to that of reference standards allowed us to further examine the distinct core-rim difference within a given tumor line and the difference between the two tumor lines with respect to this heterogeneity. The average NADH (core), Fp (rim), and Fp (mean) of the aggressive line were significantly lower than the average NADH (mean) or Fp (mean) of the indolent line. The average Fp (core) of the aggressive tumors was higher than the average Fp (mean) of the indolent tumors with borderline statistical significance ($p=0.07$). Our data also indicate that in aggressive tumors, the average NADH (core) concentration varies from the average NADH (rim) concentration only with borderline significance ($p=0.08$), whereas the average Fp (core) concentration was significantly higher than that of Fp (rim) ($p=0.02$). Thus, it was mainly the difference in Fp concentration that accounted for the distinct core-rim difference in Fp ratio observed in MDA-MB-231 tumors, with the average Fp ratio (core) being 0.81 ± 0.02 and the average Fp ratio (rim) being 0.30 ± 0.18 ($p=0.03$) (Table 1). Note that the fluorophore concentrations determined here are nominal values—i.e., fluorescence quantified without correction for hemoglobin absorption[14] and the differences of optical properties (e.g., quantum yield and light scattering constant) between the tissue and reference standards. Due to these factors, the nominal concentrations may deviate from the true tissue concentrations. However, the nominal NADH concentrations determined fall within the usual physiological range reported in the literature.[35,36] It would be of great interest to compare chemical analyses of the two fluorophores in the frozen tissue samples and correlate them with our redox imaging results. Such a correlation may help to establish a new calibration procedure for the determination of the true concentrations of the endogenous fluorophores.

Naturally, both tumor size and tumor growth rate may be considered as contributing to and/or correlating with tumor metastatic potential. Could these factors be partially responsible for the observed mitochondrial redox state difference? These two factors may be excluded from this study due to the following considerations. First, we have chosen tumors of similar size for this study. All tumors were 6 to 10 mm in diameter resulting in an average volume 173 ± 102 mm^3 for MDA-MB-231 and 165 ± 106 mm^3 for MCF-7. The size difference of the two groups was statistically insignificant ($p=0.96$). The comparable tumor size between the two lines emphasizes that the observed mitochondrial redox state difference between the two lines is caused by factors other than tumor size. However, this does not exclude the potential effect of tumor size on mitochondrial redox state. As a matter of fact, it is known that in the clinic larger tumors tend to be more aggressive than smaller ones. Their mitochondrial functions and redox states may be different as well. In the future, we can image tumors grouped into different sizes, e.g., small, medium, and large, to investigate the effect of tumor size on mitochondrial redox state and to test whether the correlation between mitochondrial redox state and tumor aggressiveness holds for tumors of different sizes. Second, regarding the growth rate of tumors in the cohorts of mice examined in these experiments, it took only 20 days for the MCF-7 tumors to grow to the desired size but 50 days for the MDA-MB-231 tumors. The growth rate of the less metastatic MCF-7 tumors was much greater than that of more metastatic MDA-MB-231 tumors. On the other hand, in our previous study of melanoma, the highly metastatic C8161 melanoma grew faster than the weakly metastatic A375P, yet the C8161 had a more oxidized Fp ratio (core) than the A375P.[27] Apparently, growth rate does not account for the difference in mitochondrial redox state observed by redox scanning as reported in the present study.

When choosing the tumor samples, we made sure that none of the tumors used in this study had an apparent necrotic center. We have also performed terminal deoxynucleotidyl transferase dUTP nick end labeling (TUNEL) assay for both the indolent and the aggressive tumors. The TUNEL assay results (Figs. 4 and 5) showed a low level of cell deaths in either of the tumor lines xenografted in nude mice. Additionally, the cores of both tumor lines had large amounts of living cells indicated by their intact nuclei stained with $4',6$-diamidino-2-phenylindole (DAPI), although the cell density in the tumor rim appeared to be higher. Similar results had been observed and reported for melanomas previously.[37]

4.2 Possible Metabolic States in Tumors

Previously, Chance and coworkers established five distinct states of the mitochondrial respiratory chain that can be distinguished on the basis of Fp and NADH levels as well as Fp redox ratio Fp/(Fp+NADH).[14,15,17] States 1 to 4 all are associated with an adequate oxygen supply. With low levels of adenosine diphosphate (ADP) and endogenous substrates, state 1 is characterized by low levels of oxidative metabolism with low Fp and high levels of NADH, and thus, a low Fp redox ratio. In state 2, mitochondria have adequate ADP but are starved of substrate, which is characterized by very high
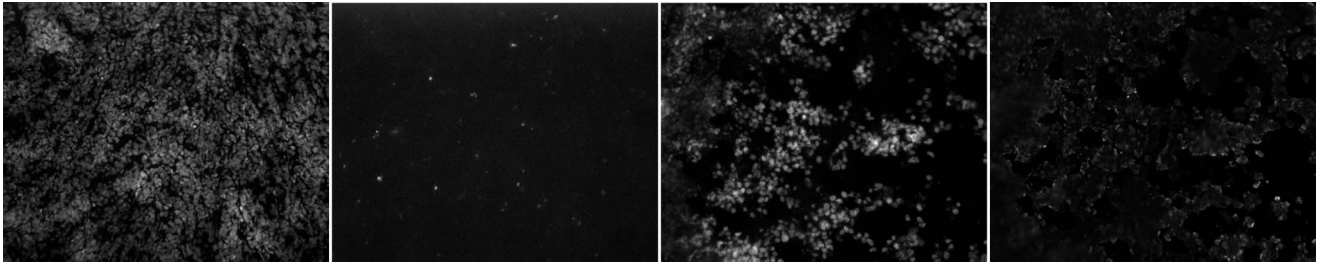
Fig. 5 TUNEL assays for tumor cell death in a representative MCF-7 tumor. From left to right: tumor rim DAPI staining, tumor rim FITC staining, tumor core DAPI staining, and tumor core FITC staining. DAPI stains the cell nucleus, and FITC stains the TUNEL positive cells (Ref. 37).

levels of Fp and low levels of NADH and, thus, a high Fp redox ratio. State 3 corresponds to adequate levels of ADP and substrate resulting in rapid oxidative metabolism, also accompanied by a high Fp redox ratio but not as high as in state 2, and lower NADH but not as low as in state 2. State 4 corresponds to a resting or metabolically inactive state with low ADP but adequate supply of substrate; mitochondria are mainly reduced with high NADH and low Fp resulting in a low Fp redox ratio. State 5 represents an anaerobic condition in which oxygen is exhausted with high levels of substrate and ADP. Mitochondria are fully reduced in state 5 with the highest NADH.

By comparing our results with the preceding redox states, we may assign the metabolic conditions of the more metastatic breast tumor core cells to state 2 or 3 because as shown in Fig. 3(b) the aggressive tumor cores have quite high Fp levels and very low NADH levels. It has been shown in certain cancer xenografts that the outer rim of the tumor is better perfused than the central region.[27,38–40] Utilizing MRI and redox scanning, our melanoma studies demonstrated a distinct core-rim difference both for the blood transfer constant (K_{trans}) measured by dynamic contrast enhancement MRI (DCE-MRI) and the mitochondrial redox state measured by low-temperature NADH/Fp fluorescence.[27] The more aggressive melanoma line appears to have a tumor core with less blood perfusion, lower nutrient supply, and a more oxidized redox state. It is possible (and, indeed, likely but not yet proven) that the central region of the aggressive MDA-MB-231 breast tumors is also poorly perfused; the cells in this region could be starving, whereas the cells in the rim are well supplied with nutrients. If this is true, then the cells in the core of the aggressive tumor are in state 2 of mitochondrial metabolism. However, since these tumors were still growing at the time of animal sacrifice, the high Fp redox ratio could also indicate that the cells in the core may have had adequate levels of ADP and substrate yielding fast oxidative metabolism—i.e., the characteristics of state 3. In the future, DCE-MRI measurement and relevant histological assays could be performed to further determine the redox state of the cells in the aggressive breast tumor core.

Mitochondrial functional/metabolic abnormalities and oxidative stress have been associated with tumorigenesis and progression to metastasis.[41,42] The result obtained in this study suggests that mitochondrial redox state could be used as a potential indicator for cancer metastatic potential. The Fp redox ratio for the aggressive breast tumor core is in the range that is observed in aggressive melanomas, and the Fp redox

ratio of the indolent breast tumor is also in the range of indolent melanomas.[27] Therefore, we are suggesting that the conclusions drawn from the more extensive melanoma study probably also carry over to breast cancer and perhaps other cancers.

4.3 Mitochondrial Redox State, Hypoxia, and Aerobic Glycolysis

Since hypoxia has been regarded as one of the driving forces for tumor progression and hypoxic tissue regions have been identified in tumors[43,44] the question naturally arises whether hypoxia might contribute to the redox state differences between the metastatic and indolent tumors and between the core and rim region in the metastatic tumors. To address this question in the future, we may measure oxygen levels in these xenografts in addition to their redox states. Nevertheless, less oxygen means more NADH, less oxidized flavoproteins and more reduced mitochondrial redox state,[25] which contrasts with what was observed in this study—i.e., the more aggressive tumors having more oxidized redox state in the tumor core. Therefore, hypoxia does not seem to explain the difference in the mitochondrial redox state we have observed in this study. Furthermore, it is noted that an oxygen concentration greater than 4 to 8 μM would saturate oxidative phosphorylation.[45] Only when oxygen level is below 1 μM can the oxidative phosphorylation be compromised to alter the mitochondrial redox ratio measured by cryogenic NADH/Fp fluorescence imaging (redox scanning). Still, it is possible that hypoxia affects mitochondrial redox state indirectly by inducing changes in gene expression of certain proteins that may affect the mitochondrial redox state. Imaging of both hypoxia and mitochondrial redox state in the same tumor will be helpful to explore the connection of hypoxia to mitochondrial redox state directly or indirectly.

Apart from hypoxia, the Warburg effect, discovered by Otto Warburg eight decades ago, may be considered for possible relevance to the results of this study. The Warburg effect is the observation that most cancer cells display elevated glucose uptake and predominantly produce energy by glycolysis rather than by oxidative phosphorylation in mitochondria, even in the presence of adequate oxygen.[46–48] The Warburg effect is the basis of the wide application of fluoro-deoxyglucose-positron emission tomography (FDG-PET) imaging to staging various types of cancers.[49,50] The mechanisms by which tumor cells possess enhanced aerobic glycolysis are still being investigated. Warburg's hypothesis[51] that

the higher glucose metabolism in cancer cells was due to the respiration of all cancer cells being damaged does not hold true for all types of tumor cells.[45,52–54] It became known that many, if not all, cancer cells showed various degrees of increase in glycolysis compared to normal tissues depending on the cell types and cell growing conditions. Some could produce more than 50% of their ATP through glycolysis,[55] whereas others, such as one of the tumor lines used in our study, MCF-7 cells, generate 80% ATP through oxidative phosphorylation.[56]

Some studies indicate that MCF-7 is less glycolytic than MDA-MB-231 *in vitro*. It is noted that under both hypoxic and normoxic conditions, the MCF-7 cells have much lower aerobic glucose consumption rates compared with the MDA-MB-231 cells.[43] It is also reported that MCF-7 cells have three times higher basal oxygen consumption rates than MDA-MB-231 cells *in vitro*.[57] This is consistent with a PET study reporting that MDA-MB-231 mouse xenografts had higher FDG uptake than MCF-7 xenografts.[58] Since it is hardly possible for PET to differentiate between the core and rim of a 6- to 10-mm tumor at an imaging spatial resolution of ~2 mm, it would be of research interest to use an optical analog of 2-deoxy-glucose (pyro-2DG) to image glucose uptake in tumors at 100-μm high resolution[59,60] and co-register it with the corresponding redox state images.

Imaging mitochondrial redox state may provide a necessary basis for a more complete understanding of the Warburg effect. The regulation of glycolysis depends on mitochondrial respiration, and respiration is probably at the basis for the tumor high glycolytic activity of the tumor.[61] A multiparameter metabolic analysis study revealed a close link between attenuated mitochondrial bioenergetic function and enhanced glycolytic dependency in certain human tumor cells.[62] It was discovered that the mutated genes in mtDNA from MDA-MB-231 cells that encoded NADH dehydrogenase subunit 6 caused a deficiency in respiratory complex I activities and that poorly metastatic tumor lines became highly metastatic tumors after receiving mtDNA from MDA-MB-231 cells.[42,63] Collectively, these observations suggest that MDA-MB-231 cells and the corresponding mouse xenografts have higher glucose metabolism due to impaired mitochondrial respiration.

However, it is unclear whether oxidized mitochondrial redox state in MDA-MB-231 observed in this study should correspond to impaired mitochondrial respiration. Our redox scanning results also revealed that the MDA-MB-231 tumor rim was not significantly different from that of MCF-7 in its mitochondrial redox state. Only the mitochondrial redox state of the core of the aggressive tumors differentiated between the two lines. Currently, redox scanning can not distinguish between extremely low respiration, i.e., starvation (state 2) and high respiration (state 3). Co-registration of redox imaging with oxygen metabolic rate in tumor tissue is needed to resolve this issue, which will be the direction of our future work. Arguably, it is also necessary to obtain 3-D co-registered information about multiple physiological parameters such as pH, pO_2, mitochondrial redox state, oxygen consumption, and glucose consumption rate in the same tumor to provide a more complete understanding of the difference between MCF-7 and MDA-MB-231 xenografts and shed more

light on the physiological/metabolic basis of tumor aggressiveness.

4.4 *Advantages of the Low-Temperature Mitochondrial Redox Imaging in Addressing Tumor Heterogeneity*

Although cell culture studies have enhanced our understanding of cancer biology, it is well known that cancer cells in tumor tissue may not exhibit the same behavior as the same cancer cells grown in culture medium. For example, MCF-7 cells are estrogen dependent *in vitro*, but 85% MCF-7 cells in tissue no longer express estrogen receptors.[58] The tissue microenvironment in tumors is different from that of cell culture. Tumor microenvironment, epigenetic modifications, and/or genetic mutations acquired during tumor progression may cause changes that are absent in cell cultures. Additionally, high intratumor heterogeneity has been well known—for instance, the heterogeneity in pO_2 and pH.[64]

Therefore, it is important to study tumor biology *in vivo* with 3-D information to obtain more realistic understanding of tumor progression to metastasis. NADH and Fp in live tissue undergo changes within seconds once the tissue is metabolically perturbed. The snap-freezing technique used in our study arrests the metabolic processes and thus preserves the natural enzymatic state and the *in vivo* metabolic state.[14] Additionally, since fluorescence of NADH and Fp at liquid nitrogen temperatures are about 10-fold stronger than at room temperature,[14,65] the signal-to-noise ratio was substantially improved. By imaging successive slices through the frozen tissue block, we were able to obtain the 3-D information on mitochondrial redox states of tumors.

Our study of human melanoma and breast cancer xenografts demonstrated that high-resolution imaging is necessary for predicting tumor metastatic potential. In human melanoma and breast tumors, there was a distinctly more oxidized (higher Fp redox ratio) tumor core region in the aggressive tumors, and it was the mitochondrial redox state in this more oxidized core region that largely differentiated the aggressive from the indolent tumors. The size of the more oxidized core region could be as small as 1 to 2 mm for a 6- to 10-mm tumor. Such tumor heterogeneity was fully addressed by the redox scanner with an in-plane high spatial resolution down to 50-μm and 20-μm tissue shaving thickness.

5 Conclusions

We report a preliminary study directed at quantitative differentiation of two breast cancer mouse xenografts with different metastatic potential using low-temperature mitochondrial redox scanning (NADH and Fp fluorescence imaging). Our results indicate that mitochondrial redox states are sensitive and quantitative biomarkers for distinguishing the more metastatic from the indolent human breast tumor mouse xenografts. The low-temperature redox scanning method can be clinically implemented on cryogenic biopsy specimens that are expected to provide highly useful information for clinical diagnosis and treatment of breast cancers. Furthermore, our mouse xenograft studies have correlated *in vivo* mitochondrial redox states with tumor metastatic potential with more metastatic melanomas and breast tumors exhibiting more oxidized states. Applying high-resolution redox imaging of mitochondrial

metabolic states to study cancer progression to metastasis may have great impact on basic cancer research and clinical management of this disease.

References

1. I. J. Fidler, "The pathogenesis of cancer metastasis: the 'seed and soil' hypothesis revisited," *Nat. Rev. Cancer* **3**(6), 453–458 (2003).
2. M. B. Sporn, "The war on cancer: a review," *Ann. N.Y. Acad. Sci.* **833**, 137–146 (1997).
3. P. T. Winnard, A. P. Pathak, S. Dhara, S. Y. Cho, V. Raman, and M. G. Pomper, "Molecular imaging of metastatic potential," *J. Nucl. Med.* **49**, 96S–112S (2008).
4. F. Dong, A. S. Budhu, and X. W. Wang, "Translating the metastasis paradigm from scientific theory to clinical oncology," *Clin. Cancer Res.* **15**(8), 2588–2593 (2009).
5. G. H. Heppner and F. R. Miller, "The cellular basis of tumor progression," *Int. Rev. Cytol.* **177**, 1–56 (1998).
6. I. J. Fidler and M. L. Kripke, "Metastasis results from preexisting variant cells within a malignant tumor," *Science* **197**(4306), 893–895 (1977).
7. I. J. Fidler and I. R. Hart, "Biological diversity in metastatic neoplasms: origins and implications," *Science* **217**(4564), 998–1003 (1982).
8. G. H. Heppner, "Tumor heterogeneity," *Cancer Res.* **44**(6), 2259–2265 (1984).
9. R. Alexandrova, "Tumor heterogeneity," *Exp. Pathol. Parasitol.* **4**, 57–67 (2001).
10. B. Quistorff, J. C. Haselgrove, and B. Chance, "High spatial resolution readout of 3-D metabolic organ structure: an automated, low-temperature redox ratio-scanning instrument," *Anal. Biochem.* **148**(2), 389–400 (1985).
11. Y. Gu, Z. Qian, J. Chen, D. Blessington, N. Ramanujam, and B. Chance, "High-resolution three-dimensional scanning optical image system for intrinsic and extrinsic contrast agents in tissue," *Rev. Sci. Instrum.* **73**(1), 172–178 (2002).
12. H. N. Xu, B. Wu, S. Nioka, B. Chance, and L. Z. Li, "Calibration of redox scanning for tissue samples," *Proc. SPIE* **7174**, 71742F (2009).
13. L. Z. Li, H. N. Xu, M. Ranji, S. Nioka, and B. Chance, "Mitochondrial redox imaging for cancer diagnostic and therapeutic studies," *J. Innov. Opt. Health Sci.* **2**, 325–341 (2009).
14. B. Chance, B. Schoener, R. Oshino, F. Itshak, and Y. Nakase, "Oxidation-reduction ratio studies of mitochondria in freeze-trapped samples. NADH and flavoprotein fluorescence signals," *J. Biol. Chem.* **254**(11), 4764–4771 (1979).
15. B. Chance and G. R. Williams, "Method for the localization of sites for oxidative phosphorylation," *Nature* **176**(4475), 250–254 (1955).
16. B. Chance and G. R. Williams, "Respiratory enzymes in oxidative phosphorylation. 4. The respiratory chain," *J. Biol. Chem.* **217**(1), 429–438 (1955).
17. B. Chance and H. Baltscheffsky, "Respiratory enzymes in oxidative phosphorylation. VII. Binding of intramitochondrial reduced pyridine nucleotide," *J. Biol. Chem.* **233**(3), 736–739 (1958).
18. B. Chance, "Pyridine nucleotide as an indicator of the oxygen requirements for energy-linked functions of mitochondria," *Circ. Res.* **38**(5 Suppl 1), I31–38 (1976).
19. B. Chance, P. Cohen, F. Jobsis, and B. Schoener, "Intracellular oxidation-reduction states *in vivo*," *Science* **137**, 499–508 (1962).
20. I. Hassinen and B. Chance, "Oxidation-reduction properties of the mitochondrial flavoprotein chain," *Biochem. Biophys. Res. Commun.* **31**(6), 895–900 (1968).
21. B. Chance, P. Cohen, F. Jobsis, and B. Schoener, "Localized fluorometry of oxidation-reduction states of intracellular pyridine nucleotide in brain and kidney cortex of the anesthetized rat," *Science* **136**(3513), 325 (1962).
22. B. Chance, N. Oshino, T. Sugano, and A. Mayevsky, "Basic principles of tissue oxygen determination from mitochondrial signals," *Adv. Exp. Med. Biol.* **37A**, 277–292 (1973).
23. B. Chance, "Optical method," *Bull. Chin. Ceram. Soc.* **20**, 1–28 (1991).
24. B. Chance, "Spectrophotometric and kinetic studies of flavoproteins in tissues, cell suspensions, mitochondria and their fragments," in *Flavins and Flavoproteins*, E. C. Slater, Ed., pp. 498–510, Elsevier, Amsterdam (1966).
25. M. Ranji, S. Nioka, N. Xu, B. Wu, L. Z. Li, D. L. Jaggard, and B. Chance, "Fluorescent images of mitochondrial redox states in *in situ* mouse hypoxic ischemic intestines," *J. Innov. Opt. Health Sci.* **2**, 365–374 (2009).
26. K. Sato, Y. Kashiwaya, C. A. Keon, N. Tsuchiya, M. T. King, G. K. Radda, B. Chance, K. Clarke, and R. L. Veech, "Insulin, ketone bodies, and mitochondrial energy transduction," *FASEB J.* **9**(8), 651–658 (1995).
27. L. Z. Li, R. Zhou, H. N. Xu, L. Moon, T. Zhong, E. J. Kim, H. Qiao, R. Reddy, D. Leeper, B. Chance, and J. D. Glickson, "Quantitative magnetic resonance and optical imaging biomarkers of melanoma metastatic potential," *Proc. Natl. Acad. Sci. U.S.A.* **106**(16), 6608–6613 (2009).
28. C. M. Balch, A. C. Buzaid, S. J. Soong, M. B. Atkins, N. Cascinelli, D. G. Coit, I. D. Fleming, J. E. Gershenwald, A. HoughtonJr., J. M. Kirkwood, K. M. McMasters, M. F. Mihm, D. L. Morton, D. S. Reintgen, M. I. Ross, A. Sober, J. A. Thompson, and J. F. Thompson, "Final version of the American Joint Committee on Cancer staging system for cutaneous melanoma," *J. Clin. Oncol.* **19**(16), 3635–3648 (2001).
29. E. A. Seftor, R. E. B. Seftor, and M. J. C. Hendrix, "Selection of invasive and metastatic subpopulations from a heterogeneous human-melanoma cell-line," *BioTechniques* **9**(3), 324–331 (1990).
30. J. M. Kozlowski, I. R. Hart, I. J. Fidler, and N. Hanna, "A human melanoma line heterogeneous with respect to metastatic capacity in athymic nude mice," *J. Natl. Cancer Inst.* **72**(4), 913–917 (1984).
31. M. J. C. Hendrix, E. A. Seftor, Y. W. Chu, K. T. Trevor, and R. E. B. Seftor, "Role of intermediate filaments in migration, invasion, and metastasis," *Cancer Metastasis Rev.* **15**(4), 507–525 (1996).
32. M. J. Hendrix, E. A. Seftor, Y. W. Chu, R. E. Seftor, R. B. Nagle, K. M. McDaniel, S. P. Leong, K. H. Yohem, A. M. Leibovitz, F. L. Meyskens Jr., D. H. Conaway, D. R. Welch, L. A. Liotta, and W. Stetler-Stevenson, "Coexpression of vimentin and keratins by human melanoma tumor cells: correlation with invasive and metastatic potential," *J. Natl. Cancer Inst.* **84**(3), 165–174 (1992).
33. A. M. Sieuwerts, J. G. Klijn, and J. A. Foekens, "Assessment of the invasive potential of human gynecological tumor cell lines with the *in vitro* Boyden chamber assay: influences of the ability of cells to migrate through the filter membrane," *Clin. Exp. Metastasis* **15**(1), 53–62 (1997).
34. H. N. Xu, B. Wu, S. Nioka, B. Chance, and L. Z. Li, "Quantitative redox scanning of tissue samples using a calibration procedure," *J. Innov. Opt. Health Sci.* **2**, 375–385 (2009).
35. R. L. Veech, "Mitochondrial bioenergetics in intact tissue," in *Mitochondria in Health and Disease*, C. D. Berdanier, Ed., pp. 65–94, Taylor & Francis, New York (2005).
36. A. K. Ghosh, D. Finegold, W. White, K. Zawalich, and F. M. Matschinsky, "Quantitative histochemical resolution of the oxidation-reduction and phosphate potentials within the simple hepatic acinus," *J. Biol. Chem.* **257**(10), 5476–5481 (1982).
37. H. N. Xu, R. Zhou, S. Nioka, B. Chance, J. D. Glickson, and L. Z. Li, "Histological basis of MR/optical imaging of human melanoma mouse xenografts spanning a range of metastatic potentials," *Adv. Exp. Med. Biol.* **645**, 247–253 (2009).
38. D. Ranney, P. Antich, E. Dadey, R. Mason, P. Kulkarni, O. Singh, H. Chen, A. Constantanescu, and R. Parkey, "Dermatan carriers for neovascular transport targeting, deep tumor penetration and improved

therapy," *J. Controlled Release* **109**(1–3), 222–235 (2005).

39. R. B. Pedley, S. A. Hill, G. M. Boxer, A. A. Flynn, R. Boden, R. Watson, J. Dearling, D. J. Chaplin, and R. H. Begent, "Eradication of colorectal xenografts by combined radioimmunotherapy and combretastatin a-4 3-O-phosphate," *Cancer Res.* **61**(12), 4716–4722 (2001).

40. D. P. Bradley, J. J. Tessier, S. E. Ashton, J. C. Waterton, Z. Wilson, P. L. Worthington, and A. J. Ryan, "Correlation of MRI biomarkers with tumor necrosis in Hras5 tumor xenograft in athymic rats," *Neoplasia* **9**(5), 382–391 (2007).

41. L. R. Cavalli and B. C. Liang, "Mutagenesis, tumorigenicity, and apoptosis: are the mitochondria involved?," *Mutat Res.* **398**(1–2), 19–26 (1998).

42. K. Ishikawa, N. Koshikawa, K. Takenaga, K. Nakada, and J. Hayashi, "Reversible regulation of metastasis by ROS-generating mtDNA mutations," *Mitochondrion* **8**(4), 339–344 (2008).

43. R. A. Gatenby and R. J. Gillies, "Why do cancers have high aerobic glycolysis?," *Nat. Rev. Cancer* **4**(11), 891–899 (2004).

44. P. Vaupel, M. Hockel, and A. Mayer, "Detection and characterization of tumor hypoxia using pO2 histography," *Antioxid. Redox Signal* **9**(8), 1221–1235 (2007).

45. R. Moreno-Sanchez, S. Rodriguez-Enriquez, A. Marin-Hernandez, and E. Saavedra, "Energy metabolism in tumor cells," *FEBS J.* **274**(6), 1393–1418 (2007).

46. Z. Chen, W. Lu, C. Garcia-Prieto, and P. Huang, "The Warburg effect and its cancer therapeutic implications," *J. Bioenerg. Biomembr.* **39**(3), 267–274 (2007).

47. J.-W. Kim and C. V. Dang, "Cancer's molecular sweet tooth and the Warburg effect," *Cancer Res.* **66**(18), 8927–8930 (2006).

48. M. G. Vander Heiden, L. C. Cantley, and C. B. Thompson, "Understanding the Warburg effect: the metabolic requirements of cell proliferation," *Science* **324**(5930), 1029–1033 (2009).

49. A. Quon and S. S. Gambhir, "FDG-PET and beyond: molecular breast cancer imaging," *J. Clin. Oncol.* **23**(8), 1664–1673 (2005).

50. M. MacManus and R. J. Hicks, "The use of positron emission tomography (PET) in the staging/evaluation, treatment, and follow-up of patients with lung cancer: a critical review," *Int. J. Radiat. Oncol., Biol., Phys.* **72**(5), 1298–1306 (2008).

51. O. Warburg, "On the origin of cancer cells," *Science* **123**(3191), 309–314 (1956).

52. R. J. DeBerardinis, J. J. Lum, G. Hatzivassiliou, and C. B. Thompson, "The biology of cancer: metabolic reprogramming fuels cell growth and proliferation," *Cell Metab.* **7**(1), 11–20 (2008).

53. B. Chance and B. Hess, "Spectroscopic evidence of metabolic control," *Science* **129**(3350), 700–708 (1959).

54. B. Chance and L. N. Castor, "Some patterns of the respiratory pigments of ascites tumors of mice," *Science* **116**(3008), 200–202 (1952).

55. R. A. Nakashima, M. G. Paggi, and P. L. Pedersen, "Contributions of glycolysis and oxidative phosphorylation to adenosine 5′-triphosphate production in AS-30D hepatoma cells," *Cancer Res.* **44**(12 Pt 1), 5702–5706 (1984).

56. M. Guppy, P. Leedman, X. Zu, and V. Russell, "Contribution by different fuels and metabolic pathways to the total ATP turnover of proliferating MCF-7 breast cancer cells," *Biochem. J.* **364**(Pt 1), 309–315 (2002).

57. D. S. Harischandra and D. Hockenbery, "Bioenergetic differences in breast cancer cell lines," in *Proc. AACR Metabolism and Cancer Conf.*, La Jolla, California, September 13–16 (2009).

58. A. Aliaga, J. A. Rousseau, R. Ouellette, J. Cadorette, J. E. van Lier, R. Lecomte, and F. Benard, "Breast cancer models to study the expression of estrogen receptors with small animal PET imaging," *Nucl. Med. Biol.* **31**(6), 761–770 (2004).

59. Z. Zhang, D. Blessington, H. Li, T. M. Busch, J. Glickson, Q. Luo, B. Chance, and G. Zheng, "Redox ratio of mitochondria as an indicator for the response of photodynamic therapy," *J. Biomed. Opt.* **9**(4), 772–778 (2004).

60. M. Zhang, Z. Zhang, D. Blessington, H. Li, T. M. Busch, V. Madrak, J. Miles, B. Chance, J. D. Glickson, and G. Zheng, "Pyropheophorbide 2-deoxyglucosamide: a new photosensitizer targeting glucose transporters," *Bioconjugate Chem.* **14**(4), 709–714 (2003).

61. B. Chance, "Was Warburg right? Or was it that simple?," *Cancer Biol. Ther.* **4**(1), 125–126 (2005).

62. M. Wu, A. Neilson, A. L. Swift, R. Moran, J. Tamagnine, D. Parslow, S. Armistead, K. Lemire, J. Orrell, J. Teich, S. Chomicz, and D. A. Ferrick, "Multiparameter metabolic analysis reveals a close link between attenuated mitochondrial bioenergetic function and enhanced glycolysis dependency in human tumor cells," *Am. J. Physiol.: Cell Physiol.* **292**(1), C125–136 (2007).

63. K. Ishikawa, K. Takenaga, M. Akimoto, N. Koshikawa, A. Yamaguchi, H. Imanishi, K. Nakada, Y. Honma, and J.-I. Hayashi, "ROS-generating mitochondrial DNA mutations can regulate tumor cell metastasis," *Science* **320**(5876), 661–664 (2008).

64. G. Helmlinger, F. Yuan, M. Dellian, and R. K. Jain, "Interstitial pH and pO(2) gradients in solid tumors *in vivo*: high-resolution measurements reveal a lack of correlation," *Nat. Med.* **3**(2), 177–182 (1997).

65. B. Zelent, T. Troxler, and J. M. Vanderkooi, "Temperature dependence for fluorescence of beta-NADH in glycerol/water solution and in trehalose/sucrose glass," *J. Fluoresc.* **17**(1), 37–42 (2007).